Geometric simulation of electro-erosion edge honing: Insights into process mechanisms

Nima Zarif Yussefian* & Philip Koshy†

Department of Mechanical Engineering, McMaster University, Canada

Abstract

A serious limitation of sink electrical discharge machining is the rapid geometric degeneration of sharp features due to localized wear. Electro-erosion edge honing is a novel process that creatively exploits this phenomenon for the edge preparation of cutting tools. This paper presents a geometric model of the process that can accurately predict the profiles of both symmetric and asymmetric edges that are prepared in the process. Numerical simulation of the model quantifies the concept of relative duty in the context of the process, and offers unique insights into process mechanisms. In particular, the critical influence of the wear ratio in determining the prepared edge being either rounded or chamfered is clarified, in consideration of the trajectory of successive discharge trains. The work further enables an understanding of the influence of initial edge defects on the processed edge, and presents guidelines for optimizing edge quality.

1 Introduction

Electro-erosion edge honing (EEEH) is a novel tool edge preparation process [1]. The process capitalizes on the inherent limitation of sink electrical discharge machining (EDM) that sharp edges on tool electrodes rapidly degenerate into a rounded shape. The principle in this process is to sink the nominally sharp edge of a ground or an as-pressed insert into an appropriate counterface material (Fig. 1a), so as to generate a rounded edge by selective thermal erosion of the material from the tool edge. Tool inserts with a complex edge profile can be prepared by using foil counterfaces (Fig. 1b), with the foil thickness determining the extent of edge rounding [2]. The process can be configured to simultaneously prepare a batch of inserts, to generate both symmetric and asymmetric edge hones, and to bring about a defined variation in the edge radius along the cutting edge.

*Currently with Sandvik Coromant, Stockholm, Sweden

†Corresponding author

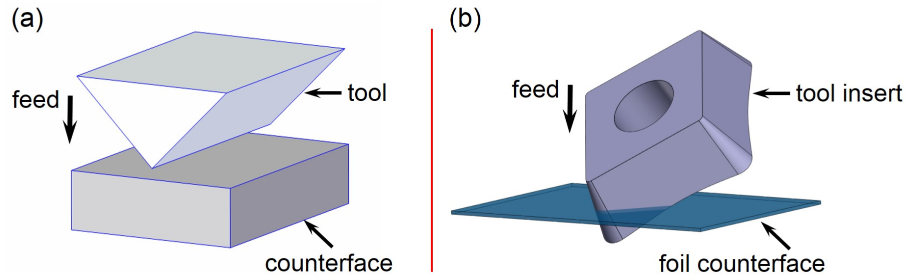

Figure 1: Principle of electro-erosion edge honing process [1, 2]. The difference in terminology between this process and conventional EDM, which is a consequence of a tool being machined in this novel process, is to be noted: the electrodes in this process shown above are referred to as the tool (that is normally the workpiece in EDM) and the counterface (which commonly is the tool in EDM).

Tool inserts may be honed in this innovative process irrespective of their hardness, as long as their electrical conductivity is sufficient for EDM. This renders it applicable to such tooling as metal-bonded polycrystalline diamond compacts that are difficult to process by mechanical means, on account of their extreme hardness. Furthermore, as the volume of material that is to be removed from the cutting edge to generate the edge hone is indeed minuscule, the relatively low material removal rate of EDM is of no detriment in this process. This aspect as well allows for the application of conservative pulse energy levels, which limits possible thermal damage to the cutting edge that can adversely influence tool life. In reference to the excellent machining precision that is characteristic of EDM, the process also corresponds to minimal variability in edge geometry [2], as compared to conventional brush honing and micro-blasting processes. This is of much industrial significance in terms of robust tool performance, which has beneficial implications when cutting high-value components.

Considering that direct experimental observation of gap phenomena in the EEEH process is difficult if not impossible, the work reported in this paper focused on applying geometric simulation to understand the process in fundamental terms. Geometric simulation of sink EDM seems to have been first reported by Tricarico et al. [3] in the late eighties to investigate the evolution of workpiece boundary in consideration of tool wear and gap width. Kunieda et al. [4] advanced this technique by modelling the tool and workpiece as mesh elements. This facilitated the integration of individual craters as basic units of material removal, with reference to discharge locations determined by the local gap width and machining debris. The model was subsequently enhanced to be applicable to profiles with fine geometric features, by incorporating the concept of relative duty, which refers to the effect of profile curvature on the local removal rate [5].

As opposed to cubic mesh elements considered in the aforementioned works, conic crater shapes have also been considered [6]. In their work on micro-EDM of blind holes, Jeong and Min [7] considered the role of local surface topography on the removal volume per spark, and were successful in employing geometric simulation for off-line tool wear compensation. Izquierdo et al. [8] considered the temperature fields in the workpiece due to superposition of multiple discharges, and on appropriate calibration of relevant parameters, were able to predict the removal rate and surface finish to within several percent of that observed experimentally. Further details on geometric simulation of EDM as well as its applications can be found in a review paper by Hinduja and Kunieda [9].

The particular objectives of this research were two-fold: (i) to gain insights into the mechanism of shape generation in the EEEH process, and (ii) to formulate a model for the quantitative prediction of the final edge geometry with reference to process/edge geometric conditions. To this end, geometric simulation was used as a tool to comprehend shape evolution of the edge with the progression of material removal, by continuously tracking the envelope of overlapping micro-craters that collectively constitute the generated edge profile. Previous experimental work [1, 2] indicated the ratio of the volume of material removed from the tool electrode to that from the counterface (defined as the wear ratio ν in the context of this new process) to play a decisive role in the micro-geometry of the prepared edge being either chamfered or rounded. It was hence of interest to apply the model to investigate the influence of the wear ratio, and to clarify the mechanism behind such an intriguing transition that is of practical relevance. In addition to understanding this phenomenon, the application of the model in comprehending the variability in the micro-geometry of the prepared edges was also investigated.

2 Simulation

2.1 Methodology

Simulation of the EEEH process was undertaken in a two-dimensional plane, with the cutting edge and counterface modelled as two arrays of equispaced nodes. The simulation technique referred to geometric (tool wedge angle, initial edge radius, foil thickness) and process (gap width, crater geometry) parameters. The material removed per discharge was assumed to be constant, with information on the crater geometry and gap width required for the simulation obtained experimentally.

The location of discharges in EDM is non-deterministic, and is dependent on the local dielectric strength determined by the level of gap contamination, and the imposed field intensity [10]. Given that typical edge radius values are on the order of only a few tens of μm and that the process refers to conservative pulse parameters, the volume rate of debris generation in EEEH is negligibly small as compared to conventional EDM processes. This combined with the fairly open process geometry facilitates rapid and even dispersal of the gas bubbles and the machining debris. Discharges were hence assumed to occur across a gap (that is nominally of an even width) at locations that correspond to the shortest distance between the tool and the counterface, with no consideration for the debris field.

The feed motion in the process was simulated by moving the tool towards the counterface such that the gap width was maintained within limits that correspond to the nominal value measured experimentally. Material removal was thereafter simulated at nodes on the tool and counterface that correspond to the minimum distance between the tool and the counterface (called the sparking nodes). This cycle was repeated to the completion of the process. Crater profiles were assumed to be a segment of a circle, with width w and depth d (Fig. 2a) such that the radius of curvature R is given by $[(w^2 + 4d^2)/8d]$. The corresponding crater area A_c in the plane of the 2D simulation can be calculated as:

$$A_c = R^2 \cos^{-1}\left(\frac{R-d}{R}\right) - (R-d)\sqrt{2Rd - d^2} \tag{1}$$

A_c was measured experimentally for the tool and counterface, as detailed later in Section 2.2. Craters were also considered to be oriented perpendicular to the spark with the sparking nodes located on the axes of symmetry. The spark orientation was defined by the angle θ with respect to the horizontal (Fig. 2a). In order to adequately capture the crater geometry in the simulation, the node spacing was such that a single crater spanned several nodes, Fig. 2b. With the profile of the crater section readily computed, the coordinates of the tool and the counterface were updated after every discharge, as illustrated in Fig. 2b.

On iterating this step to simulate overlapping craters from successive discharges, the effect of the curvature and topography of the generated profile has to be adequately considered. For instance, referring to Fig. 2c, the material removed in the second discharge is smaller than in the first one, and is also smaller than the reference crater area A_c calculated using eqn. 1 due to the local topography of the profiles.

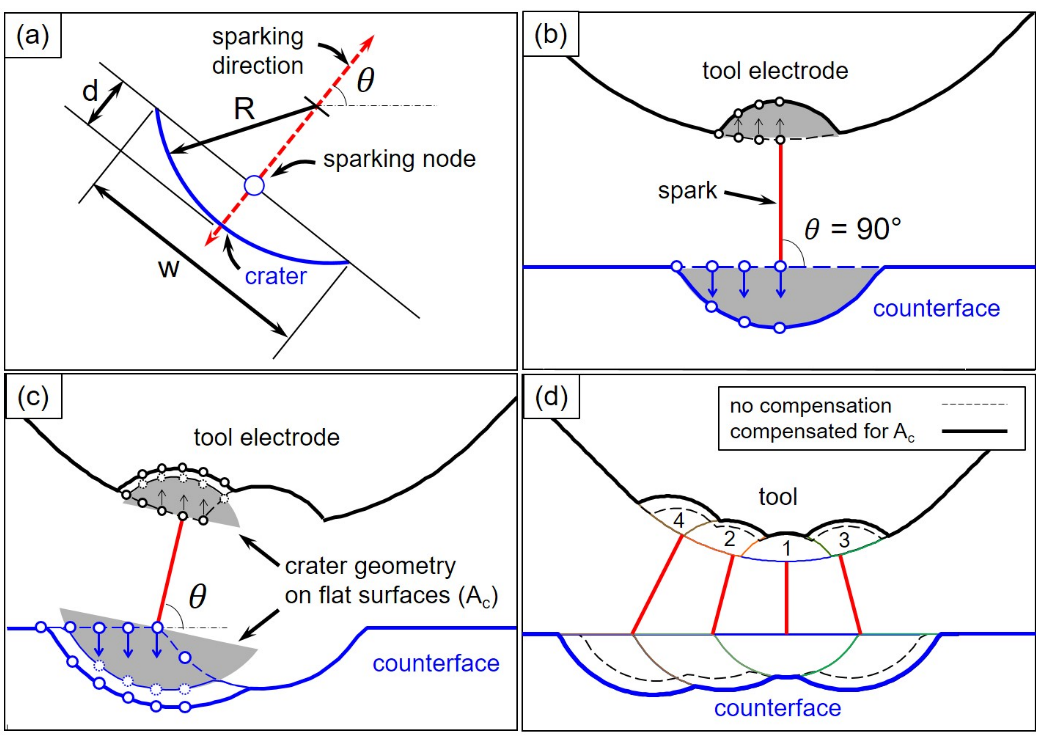

Figure 2: Simulation methodology.

The width and depth of the craters were hence proportionally incremented such that the material removed in each discharge corresponds to A_c, for both the tool and the counterface. This will in turn secure the correspondence between the simulated and measured wear ratio. For the first few sparks, the profiles of overlapping craters simulated with this methodology is shown in Fig. 2d.

2.2 Experimental details and model calibration

Geometric simulation of the EEEH process necessitates empirical information on such parameters as the wear ratio, gap width and crater geometry, which depend on the pulse parameters, polarity and the electrode/counterface materials. EEEH experiments involved an oil-based dielectric fluid, an aluminum counterface of negative polarity, a pulse on-time of 0.4 μs, a pulse off-time of 1.12 μs, an average gap voltage of 50 V, and a pulse current of 1.2 A. The corresponding wear ratio was measured to be 0.4 through fine weight measurements. A gap width of 15 μm was estimated post-machining by identifying the offset at which the curvilinear profile of the tool matched appropriately with that of the counterface (on validating the simulation, the sensitivity of the edge geometry on the gap width was evaluated: the percentage difference in the radius of the processed edge was found to be similar to the percentage difference in the gap width). The tool wedge angle was 90°, and the unprepared edges referred to an initial edge radius of 5 μm.

The geometry of craters generated in single spark tests do not adequately represent those from successive discharges due to the effect of bubbles and debris particles in the working gap [8]. Measurements therefore referred to individual isolated craters on polished surfaces, which could be identified at the periphery of the machining zone that comprised several overlapping craters from a train of discharges (Fig. 3). Using a sample size of 25, the average crater width w was measured using a high resolution optical microscope to be 8.2 μm and 14 μm for carbide and aluminum, respectively; the respective average crater depth d was measured to be 1.7 μm and 2.3 μm.

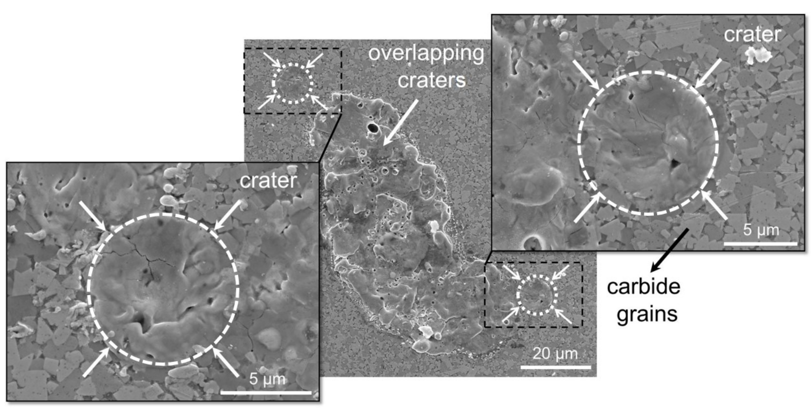

Figure 3: Micrographs of craters on the carbide surface.

2.3 Validation

The numerical simulation methodology presented above was validated by comparing the edge radii calculated from simulated profiles with those measured on prepared cemented carbide edges, as a function of the thickness of the foil counterface used to hone the edges. A further validation involved a comparison of the simulated and measured edge profiles themselves, for both symmetric and asymmetric edges.

Fig. 4 presents a comparison of the experimentally measured edge radius values against those obtained from simulation, for various foil thickness. Experimental values (shown as data points) can be seen to be somewhat higher, with the maximum error being about 14%, at the lower end of foil thickness. The error decreases progressively with increasing foil thickness to less than 1% for the edge radius of 53 μm. This is due to microscopic defects such as edge-chipping being progressively less of a relative consequence in terms of the finished edge geometry, with an increase in the volume of material removed from the edge. This will be discussed in detail in Section 3.3.

Figs. 5a and 5b show the extraordinary conformance between the simulated and measured profiles of a symmetric and an asymmetric edge, respectively; this validates the capability of the simple geometric simulation in predicting the profile of even an asymmetric edge with remarkable accuracy. Fig. 5b further presents experimental proof for the capability of the EEEH process in generating asymmetric edges for the first time; in this instance, the edge was prepared by tilting it through 20° to the feed direction, such that more material is removed from one face of the tool relative to the other.

In investigating tool shape degeneration in die sinking, experiments of Crookall and Moncrieff [11] indicated rounding of sharp corners to involve mechanisms other than geometry, when the radius of curvature of the tool electrode was less than about 3 mm. They attributed this to the sharp edge affecting the flow field of the dielectric which in turn could lead to uneven gap-widths along the tool profile due to non-uniform debris concentration, and the edge being subject to isolated thermal and shock wave effects. The fact that the present simulation accurately predicts the edge profile based on geometry alone points to such extraneous effects to be of little

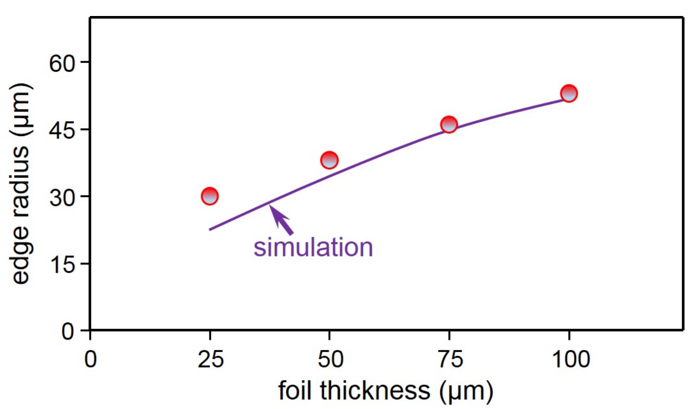

Figure 4: A comparison of simulated and measured edge radii.

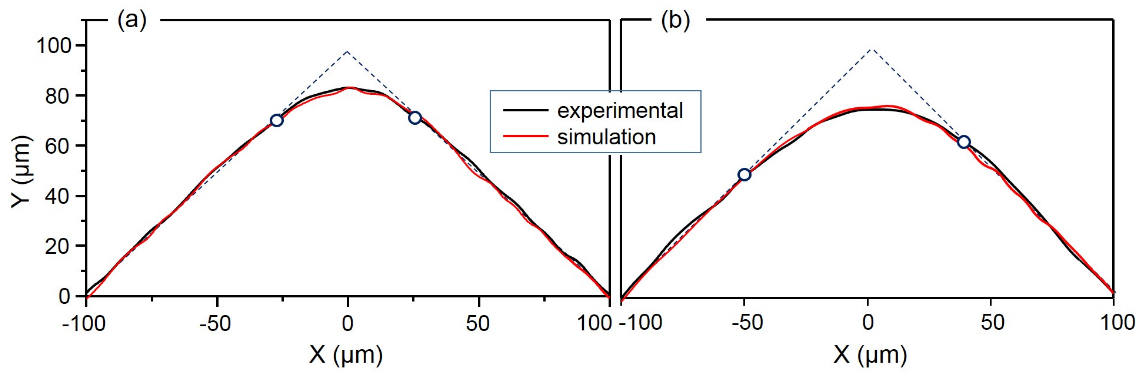

Figure 5: Simulated and measured edge profiles.

consequence in the EEEH process. This is not surprising in light of the low pulse power and the low volume rate of material removal in the generation of a honed edge.

3 Insights from simulation

On validating the simulation technique, it was used to gain insights into EEEH process mechanisms, a discussion of which follows.

3.1 Characteristics of localized edge wear

The phenomenon that is at the core of the EEEH process is the rapid geometric degeneration of features with a large curvature in sink EDM due to localized wear. Considering the detriment this phenomenon poses to the accuracy of machined components in practical die sinking applications, Crookall and Moncrieff [11] proposed the concept of relative duty to investigate this. Referring to the curvilinear section of the tool and the counterface shown in Fig. 6, the ratio of the rate at which material

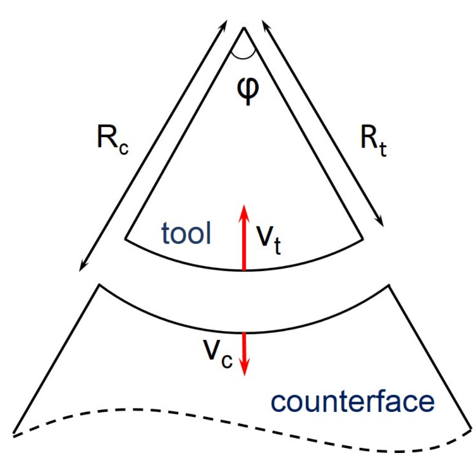

Figure 6: Concept of relative duty.

is removed from the tool to that from the counterface called the wear ratio ν can be written as $(\varphi R_t V_t/\varphi R_c V_c)$ where R is the radius of curvature and V signifies the rate at which the tool and counterface surfaces recede in the radial direction; subscripts t and c refer to the tool and counterface, respectively. For a given wear ratio, when R_t is less than R_c (representing a convex tool as shown in the figure), the recession of the tool surface per unit time V_t has to be proportionally higher than that of the counterface V_c. This represents a higher wear of the tool relative to the counterface.

The numerical simulation developed in this work allows for the quantification of the concept of relative duty, in terms of the discharge density, which is the number of discharges per unit length of the cutting edge (for a two-dimensional simulation). It may be noted that the discharge density is dependent on such variables as the counterface thickness and the spatial resolution at which the simulation is run, but it is valuable for the purpose of a comparison between edges of different geometry in this instance. Figs. 7a and 7b show the distribution of the discharge densities along the cutting edge, for tools with initial edge radii of 5 μm and 50 μm, respectively. The values at each section of the edge have been integrated over the duration of the process for a counterface thickness of 50 μm. The figure clearly shows the smaller initial edge radius to refer to a higher peak discharge density, which is consistent with the notion of relative duty.

Mapping the computed discharge density in Fig. 7b (initial edge radius of 50 μm) to individual domains on the prepared cutting edge shows the highest density to cor-

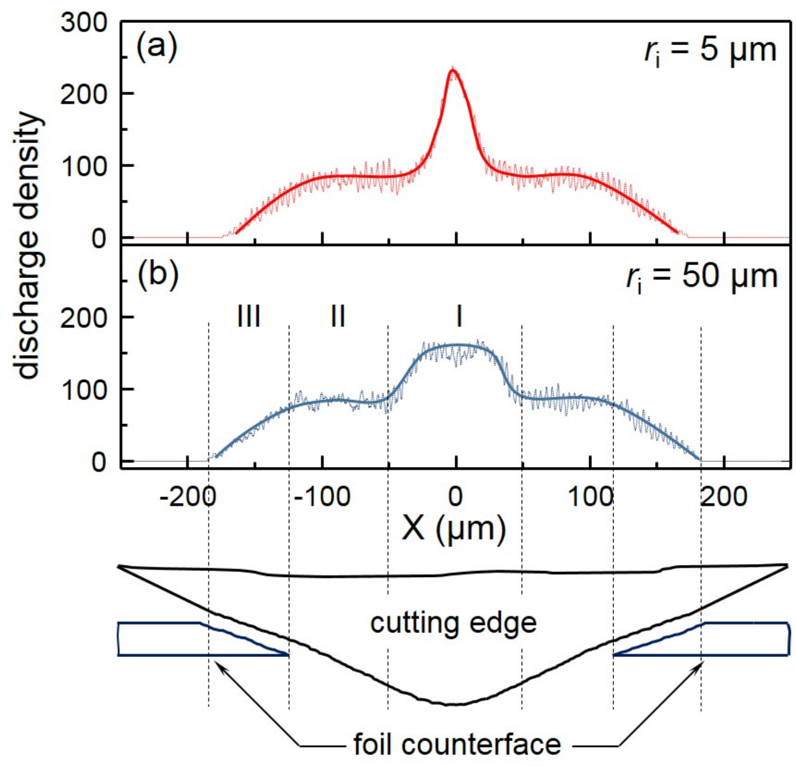

Figure 7: Spatial discharge density distribution.

respond to the tip of the cutting edge (domain I) with the largest curvature. Domain II refers to a density that is largely constant on account of this section referring to zero curvature; during the course of the edge having sunk past the thin counterface, this segment of the tool edge has been subject to an identical erosion history. The nearly linear change in the discharge density in domain III is an indication of this section of the edge in the process of being eroded, as it feeds into and through the counterface.

Considering the significant dependence of the rate of erosion on the instantaneous tool curvature, Fig. 8 shows the ratio of the final edge radius r_β to the initial edge radius r_i as a function of r_i, for various counterface (foil) thickness. The data serves as a guideline for the selection of an appropriate counterface thickness, in the honing of a cutting edge of a known initial radius to a target edge radius. Interestingly, it is evident that the EEEH process is better suited for the rapid preparation of edges with an initial edge radius that is less than about 10–15 μm, which is the range in which most ground and as-pressed edges fall into. Honing of edges with a higher initial edge radius correspond to diminishing returns: for tools with an initial edge radius of about 25 μm or higher, the increase in edge radius is relatively minimal, and is largely independent of the counterface thickness; fortunately, such edge radius values are not relevant in practice.

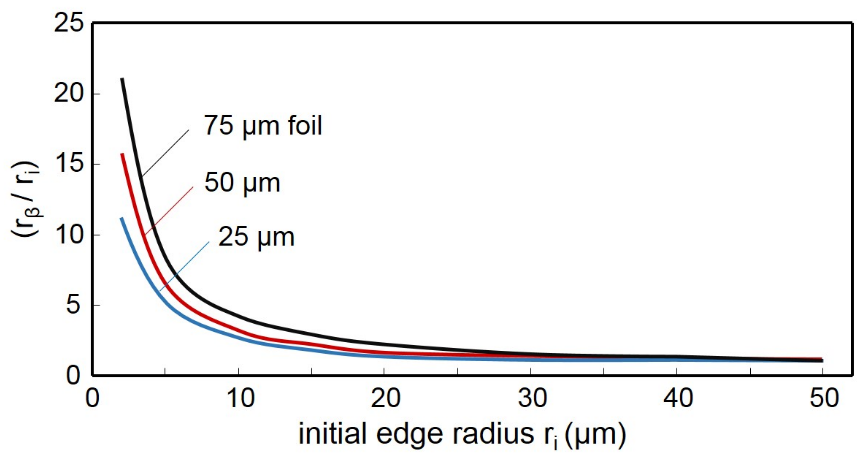

Figure 8: Effect of initial edge radius r_i on the final edge radius r_β.

3.2 Effect of wear ratio on edge geometry

An intriguing aspect of the EEEH process is that the geometry of the generated edge is dependent on the wear ratio ν [2]. Fig. 9 shows three-dimensional surface representations as well as cross-sectional views of cemented carbide edges that were electro-erosion honed experimentally under wear ratios of 0.15, 0.4 and 5.0. Such a large variation in the wear ratio was realized by changing the material of the counter-face (aluminum and copper) and the polarity in the edge honing experiments. At the lower end of the wear ratios investigated (0.15), the edge is dome-shaped (Fig. 9a)

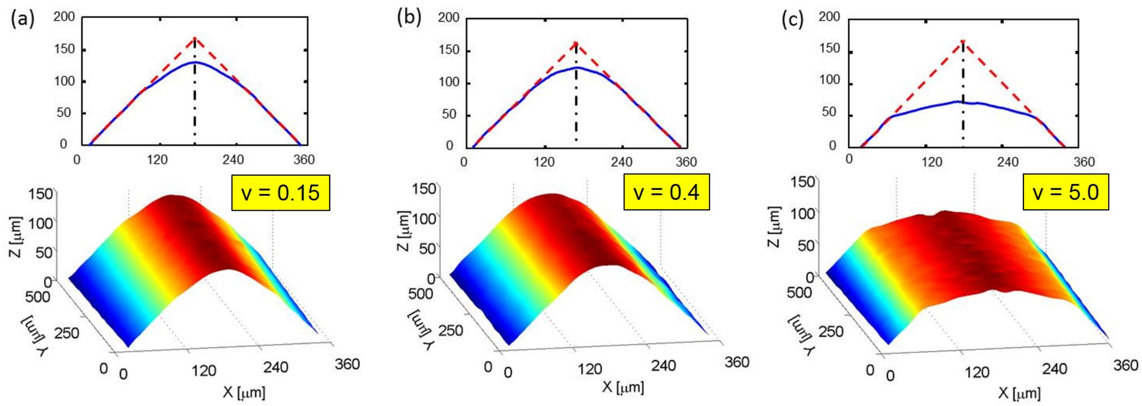

Figure 9: Effect of wear ratio on edge shape [2].

which implies that relatively more material has been removed locally from the rake and flank faces, which is undesirable. At the other end (wear ratio of 5.0), the edge appears chamfered rather than rounded (Fig. 9c). At the intermediate wear ratio of 0.4, the edge is appropriately rounded (Fig. 9b).

It is clear from this figure that the wear ratio is a critical parameter that wields a significant influence on the microgeometry of the edge, and that by simply changing the wear ratio, both rounded and chamfered edges could be generated. It is hence of interest to understand the mechanism of shape generation in EEEH, with particular reference to the wear ratio. To this end, its effect was simulated by changing the crater area on the counterface (at a constant aspect ratio), with the crater geometry on the tool edge left unaltered, such that the wear ratios correspond to 0.15, 0.4 and 5.0.

The left panel in Fig. 10 shows the evolution of discharge orientation angle θ (as defined in the Fig. 2) for the first 250 discharges, as obtained from numerical simulation. The right panel shows the corresponding histograms derived from samples comprising 1000 discharges. At a high wear ratio of 5.0, the angle can be seen to be normally distributed, with the bulk of the values in the narrow range between 80° and 100°. This indicates that the discharges are largely vertical as the discharge location traverses back and forth in the gap space. The envelope of such discharges corresponds to an approximately linear trajectory, which should be expected to generate a chamfered edge, as is observed experimentally in Fig. 9c.

This contrasts significantly with the distribution corresponding to a wear ratio of 0.15, wherein the discharge orientation is bimodally distributed, and is seen to cluster around 45° and 135°. Given that the wedge angle of the tool is 90°, these angles represent normals to the flank and rake faces of the tool, and hence refers to localised material removal at either end of the cutting edge on the rake and flank faces, which generates an undesirable dome-shaped edge (see Fig. 9a). Such a clustering of discharges is clearly unfavourable in the generation of an edge with a constant curvature.

With an increase in the wear ratio to 0.4, it is clear that the discharge orientation

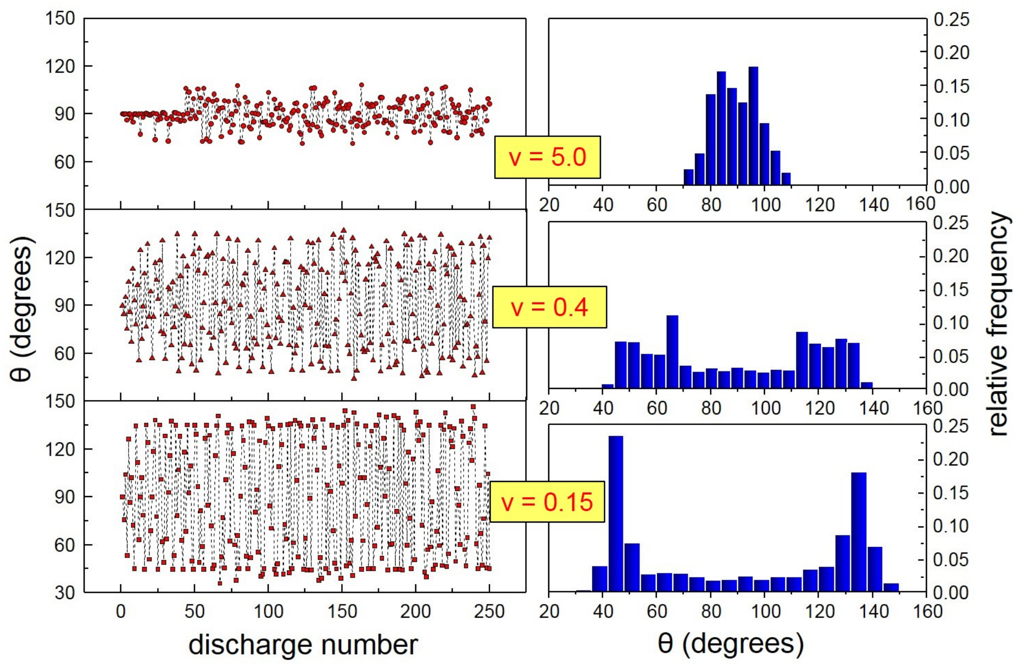

Figure 10: Effect of wear ratio on the evolution and distribution of discharge orientation.

tends to approach more of a uniform distribution between about 45° and 135°. Such a distribution points to a sweeping motion of the discharges along a circular trajectory in the annular gap space, which would indeed generate the desirable rounded shape. It is very intriguing to note that successive sparks can be made to traverse an arc of a circle by appropriately tuning the wear ratio in the EEEH process, which entails just a simple one-dimensional process kinematic of sinking the tool into the counterface, with no need for any intricate alignments. The mechanical equivalent of generating such fine radii would be fairly demanding; in the preparation of honed edges using path-controlled operations such as grinding, the curvature would indeed have to be approximated by several linear segments [12].

The mechanism behind the linear and radial trajectory of successive discharges at high and optimal wear ratios resulting in chamfered and honed edges can further be visualized with reference to a schematic model shown in Fig. 11. The top panel in the figure refers to three successive discharges (from left to right) at a high wear ratio of 5, which corresponds to significantly more material removed off the tool, relative to the counterface. The spatial location of each of the three successive discharges is determined by the shortest distance between the tool and the counterface across the spark gap after every discharge, with the shaded regions signifying material that is removed. In each case, it can be seen that the discharge orientation is 90°, which conforms to what was observed in the simulation (Fig. 10a). The discharge trajectory is therefore largely horizontal, which generates a chamfered edge. Generation of the chamfer can also be rationalized by considering that at a high wear ratio there is

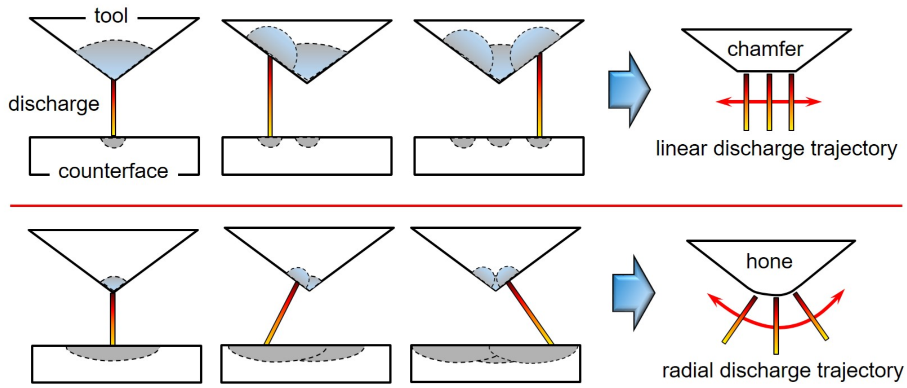

Figure 11: Shape generation of honed and chamfered edges.

relatively little material removed from the counterface, with the consequence that the prepared segment of the wedge shaped tool would tend to assume the shape of the flat counterface, which results in a chamfer.

At a wear ratio of 0.4, on the other hand, relatively more material is removed from the counterface (lower panel in Fig. 11), and consequently the second and third discharges, as determined the closest distance between the tool and the counterface, refer to oblique orientations as shown. The corresponding trajectory of the discharges will therefore be radial, the envelope of which would generate a honed edge. This in essence again represents the simplicity of the electro erosion edge honing process, wherein both honed and chamfered edges may be prepared by just tuning the wear ratio, and the integrity of the prepared tool surface can be controlled by employing an appropriate pulse energy. In perspective, the large number of parameters that need be controlled in processes such as micro blasting and brushing render them difficult to control and prone to much variability in the process response [13].

3.3 Variability in edge geometry

Although EDM in itself is a precise process, variability in the geometry of the prepared edge can arise from such defects as edge chipping that is possibly induced during grinding of tool edges prior to edge preparation. Such variability could manifest along the same edge as well as between edges. It is hence of interest to examine the effect of such initial edge defects on the geometry of edges prepared in the EEEH process. To this end, simulations were first run to study the evolution of the geometry of an edge with and without edge chipping.

Fig. 12a shows a pristine edge (with an initial edge radius of 5 μm) to correspond to an edge radius of 26 μm after EE-honing. The corresponding edge radius is 29 μm, when the edge had a chipping (Fig. 12b), which represents a variability of over 10% in the edge radius. It is interesting to note that the chipping has little influence on the form (roundness) of the edge, once the chipping has been entirely mitigated (which would bring about an enhanced tool performance). With additional processing time, the difference in the edge radius between the pristine (Fig. 12c; 47 μm) and the

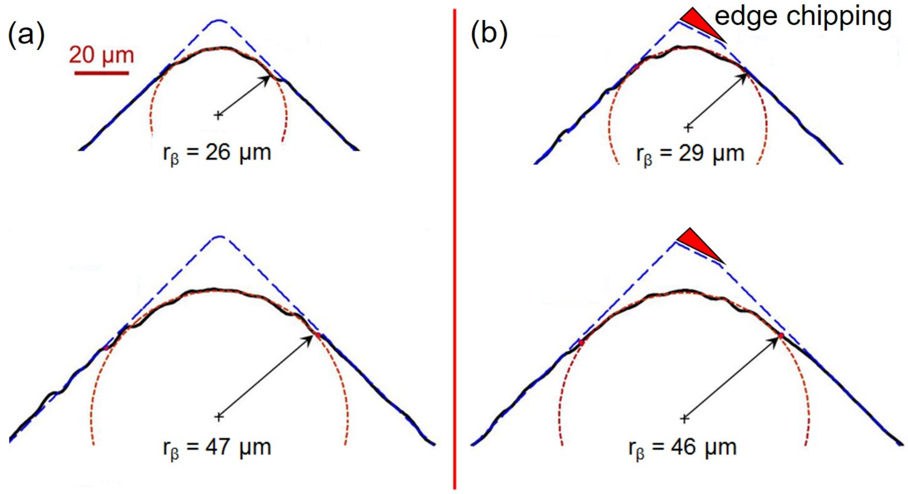

Figure 12: Effect of chipping on the generated edge geometry.

chipped edge (Fig. 12d; 46 μm) is indeed negligible.

In consideration of the strong dependency of the edge radius on the incoming condition of the unprepared edges, Fig. 13 shows the maximum variability along a cutting edge, with respect to the length and orientation of chipping, for two values of counterface foil thickness. For a given foil thickness, the maximum variability is obtained as the difference between the edge radius values corresponding to a section that is pristine and the one that has sustained edge chipping (this assumes that there is at least one section along the edge that is devoid of any chipping). In the case of pristine edges, EE-honing using foils of thickness 50 μm and 100 μm will result in edge radii of 35 μm and 52 μm, respectively (see Fig. 4).

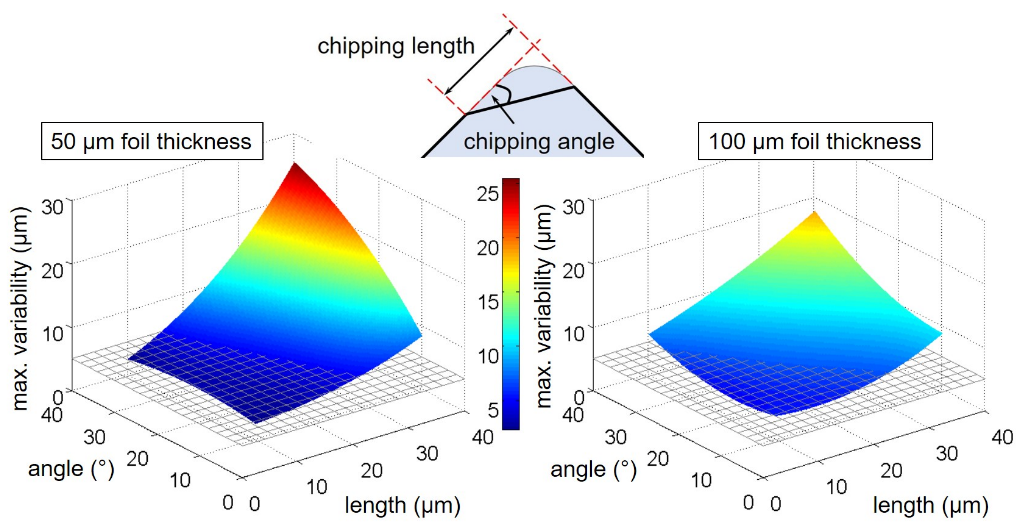

Figure 13: Maximum variability in the generated edge geometry in terms of chipping angle and chipping length.

For either foil thickness, the response surfaces obtained through simulation shown in Fig. 13 indicate the variability to increase with both chipping length and chipping angle. A very strong interaction between the chipping length and orientation is also evident, especially for the lower foil thickness. The response surfaces further help identify the combinations of maximum chipping lengths and chipping angles that may be deemed acceptable in the unprepared edges for a given edge radius tolerance (by considering the intersection of the response surface and a plane parallel to the angle-length plane that refers to a set tolerance, say 5 μm as shown in the figure). For a given chipping geometry, the figure further shows the variability to be minimized when using a thicker counterface foil, albeit the quality enhancement can be seen to be not proportional. Similar to edge chipping in ground inserts, the presence of flash in as-pressed inserts represents defects that can lead to edge radius variability along a cutting edge. The effect of such defects was also simulated, and the variability was found to be on the same order as that shown in Fig. 13, for equivalent flash geometry. The presence of flash may however be noted to correspond to an effect that is opposite to that of a chipped edge (incidence of flash reduces the edge radius at that section), as it refers to extraneous material on the edge rather than material lost due to chipping.

4 Conclusions

The paper presented a simple numerical model of the electro-erosion edge honing process. In consideration of experimentally measured crater geometry and gap width, numerical simulation of the model was shown to accurately predict the profiles of both symmetric and asymmetric prepared edges, and the edge radius as a function of the foil thickness. The work helped quantify the notion of relative duty in terms of the local discharge density, which indicated the rounding effect to be influenced by just the curvature of the edge. With reference to the processing time, the simulation indicated the EEEH process to be better suited for the preparation of edges with an initial edge radius of less than about 15 μm, which aligns with typical industrial requirements.

The model also indicated the trajectory of successive discharges to be determined by the wear ratio, which in turn had an influence on the edge being either chamfered or honed. The simulation helped visualize the generation of the rounded edge to be a consequence of the sweeping motion of the discharges along a circular arc, when using the optimal wear ratio. The model further provided insights into the role of initial edge defects on the variability in the edge radius of the honed tool, and helped determine the extent of acceptable edge chipping for a given edge radius and the associated tolerance. The simple numerical process simulation was found to be an indispensable tool for gaining insights into the process as well as for process design, the equivalent experimental approach of which would either be difficult/impossible or prohibitively time- and effort-intensive.

Acknowledgements

This work was funded by AUTO21 Canadian Network Centre of Excellence, and the Natural Sciences and Engineering Research Council of Canada.

References

[1] N.Z. Yussefian, P. Koshy, S. Buchholz, F. Klocke, Electro-erosion edge honing of cutting tools, CIRP Annals–Manufacturing Technology 59 (2010) 215–218.

[2] N.Z. Yussefian, P. Koshy, Application of foil electrodes for electro-erosion edge honing of complex-shaped carbide inserts, Journal of Materials Processing Technology 213 (2013) 434–443.

[3] C. Tricarico, R. Delpretti, D.F. Dauw, Geometrical simulation of the EDM die-sinking process, CIRP Annals–Manufacturing Technology 37 (1988) 191–196.

[4] M. Kunieda, W. Kowaguchi, T. Takita, Reverse simulation of die-sinking EDM, CIRP Annals–Manufacturing Technology 48 (1999) 115–118.

[5] M. Kunieda, Y. Kaneko, W. Natsu, Reverse simulation of sinking EDM applicable to large curvatures, Precision Engineering 36 (2012) 238–243.

[6] Y. Zhao, X. Zhang, X. Liu, K. Yamazaki, Geometric modeling of the linear motor driven electrical discharge machining (EDM) die-sinking process, International Journal of Machine Tools & Manufacture 44 (2004) 1–9.

[7] Y.H. Jeong, B.K. Min, Geometry prediction of EDM-drilled holes and tool electrode shapes of micro-EDM process using simulation, International Journal of Machine Tools & Manufacture 47 (2007) 1817–1826.

[8] B. Izquierdo, J.A. Sanchez, S. Plaza, I. Pombo, N. Ortega, A numerical model of the EDM process considering the effect of multiple discharges, International Journal of Machine Tools & Manufacture 49 (2009) 220–229.

[9] S. Hinduja, M. Kunieda, Modelling of ECM and EDM processes, CIRP Annals–Manufacturing Technology 62 (2013) 775–797.

[10] K. Morimoto, M. Kunieda, Sinking EDM simulation by determining discharge locations based on discharge delay time, CIRP Annals–Manufacturing Technology 58 (2009) 221–224.

[11] J.R. Crookall, A.J.R. Moncrieff, A theory and evaluation of tool electrode shape generation in electro discharge machining, Procs. Instn. Mech. Engrs 187 (1973) 51–61.

[12] B. Denkena, J. Kohler, C.E.H. Ventura, Customized cutting edge preparation by means of grinding, Precision Engineering 37 (2013) 590–598.

[13] B. Denkena, D. Biermann, Cutting edge geometries, CIRP Annals–Manufacturing Technology 63 (2014) 631–653.